Nanoporous gold thin films synthesised via de-alloying of Au-based nanoglass for highly active SERS substrates

(Article begins on next page)

07 July 2024

Nanoporous gold thin film prepared by chemical de-alloying of Au-based nanoglass for highly active SERS substrate

Yanpeng Xue[1]*, Eirini Maria Paschalidou[1], Paola Rizzi[1], Livio Battezzati[1]
Pierre Denis[2]*, Hans-Jörg Fecht[2]

[1]Dipartimento di Chimica e Centro Interdipartimentale NIS (Nanostructured Surfaces and Interfaces), University of Turin, Via Pietro Giuria 7, 10125 Torino, Italy
[2]Institute of Micro and Nanomaterials, University of Ulm, Albert-Einstein-Allee 47, 89081 Ulm, Germany
*Corresponding Author: xueyanpeng789@163.com; pierre.denis@uni-ulm.de

Abstract:

Nanoporous gold (NPG) thin film has been prepared by chemical de-alloying of Au based nanoglass with nanocolumnar structure, $Au_{40}Cu_{28}Ag_7Pd_5Si_{20}$(at.%), which was prepared by magnetron sputtering. By adjusting the de-alloying parameters, gold ligaments ranging from 20 to 100 nm can be obtained. The nanoporous structure of the de-alloyed thin films was characterized by SEM, TEM and XRD techniques. Surface enhanced Raman scattering of NPG thin film as substrate was investigated using Rhodamine 6G (R6G). It was found that the SERS enhancement is attributed to the localized surface plasmons within the main microstructural features with interconnected ligaments, surface grooves and defects.

Keywords: Nanoporous gold thin film; Chemical de-alloying; nanoglass; Raman spectroscopy

1. Introduction

Surface enhanced Raman scattering (SERS) has recently attracted much research attention for providing the detection of specific molecules in chemical and biological systems through their unique vibrational fingerprints[1,2]. Single molecule detection can be achieved by using plasmonic metallic nanostructures to amplify the Raman scattering of targeted molecules[3,4]. The dramatic SERS enhancement primarily arises from the localized surface plasmon resonance, i.e., light-driven collective oscillations of conduction electrons, in the close vicinity of the metallic nanostructures[5,6]. Until now, various methods have been used to prepare SERS active substrates, such as seed mediated growth of metal nanoparticles having complex shape [7], self organization to achieve controlled assembly[8] and electron-beam lithography to make periodical micropillar arrays [9]. In addition, nanoporous metals prepared by de-alloying method have been exploited as SERS active substrates[10,11]. The interesting plasmonic properties of nanoporous metals originate from their unique feature, such as nanoscale ligaments and nanopore channels within three dimensional bicontinuous porous structures[12].

De-alloying is a selective corrosion method where the less noble elements of the precursor are dissolved, while the more noble elements reorganize into an interconnected ligament/pore network by surface diffusion[13,14]. The de-alloying technique has proved to be an effective method in synthesizing three-dimensional nanoporous metals, including Au[15,16], Ag[17], Pt[18] and Cu[19].

Metallic glasses are usually multi-component materials produced by rapid solidification from their melt to bypass crystallization[20]. They are regarded as supersaturated solid solutions with high chemical homogeneity and their amorphous microstructure is free from grain boundaries and large-scale phase segregations[21]. This unique structure is attractive to obtain a uniform nanoporosity by the de-alloying method. Actually, previous reports showed that the de-alloying of amorphous ribbons gave porous self-standing materials made of Au ligaments constituted by fine crystals containing residual trapped solute elements, e. g. Ag and Pd[20,22]. Nanoglass, as a new kind of metallic glass proposed by Jing et al[23], consists of nanometer sized glassy grains separated by glassy interfaces[24] of reduced density with respect to the density of the bulk glass[25]. In our previous work, we demonstrated that the Au based nanoglass thin film exhibits a higher de-alloying rate compared with homogeneous metallic glass thin film under the same de-alloying conditions. The nanoglass peculiar structure facilitates the dissolution of less noble elements [24].

Recently, nanoporous gold thin films were fabricated by de-alloying method from sputter-deposited Au-Cu and Au-Ag crystalline precursors aiming at exploiting catalytic properties, microfabrication compatibility and excellent thiol-gold chemistry [26–28]. The applications of nanoporous gold thin films in electrochemical biosensors [29] and molecular release[30,31] was demonstrated and nanoporous gold disks fabricated by the combination of lithographic and de-alloying method[32,33] displayed high performance SERS activity[34,35]. In this study, the Au-based nanoglass thin film with nanocolumnar microstructure was deposited by magnetron sputtering at 10 Pa of Ar working pressure. Then, the chemical de-alloying of the thin film was systematically studied at various conditions. Finally, the SERS capability of nanoporous gold thin film were characterized using Rhodamine 6G (R6G) as probe molecules.

2.Methods

Au-based nanoglass thin film was deposited from a 5 cm diameter crystalline target with nominal composition $Au_{40}Cu_{28}Pd_5Ag_7Si_{20}$(at.%) selected for its good glass forming ability[36]. The master alloy was induction melted and the target was cast in a graphite mould at PX Services, La Chaux-de-Fonds (CH). Thin films were deposited by DC magnetron sputtering with a working distance of 4.5 cm and a discharge power of 30 W. Before deposition, a background pressure below 10^{-4} Pa was reached in the sputtering chamber. The substrates were cover glasses of dimension 24×24 cm. An intermediate adhesive layer of Cr, around 5 nm thick, was deposited on the substrate. A Au layer, around 50 nm thick, was then deposited on top of the Cr layer to prevent the corrosion of Cr during de-alloying. Finally, the metallic glass was deposited on top of the Au

layer. The deposition occurred at 10 Pa of working pressure of Ar and lasted for 5 min to reach a thickness of around 350 nm. The metallic glass thin film retained the same composition as the target, as it was confirmed by the energy dispersive X-ray (EDX) measurements.

Chemical de-alloying of the thin films was conducted in different HNO_3 concentrations of 1, 2, 5 and 10 M. To investigate the microstructure evolution, different de-alloying times of 5, 10 and 30 min, 1, 2, and 6 h were applied. Chemical de-alloying was also performed as a function of temperature in 1 M HNO_3 for 30 min. After de-alloying, the samples were rinsed with distilled water and then dried for investigation. XPS measurements were performed using Mg Kα (1253.6 eV) radiation (PHI 5800 MultiTechnique ESCA System, Physical Electronics), with a detection angle of 45°, using pass energies at the analyzer of 29.35 and 93.9 eV for detail and survey scans, respectively. the surface of the ligaments was etched for 10 min at a sputtering rate of 1 nm/min prior to the measurements.

The surface morphology of the thin films, before and after de-alloying, was observed by scanning electron microscopy (SEM), and their compositions were checked by Energy Dispersive X-ray Spectroscopy (EDS) after Co calibration. The structure of the material before and after de-alloying was characterized by glancing angle X-ray diffraction (GAXRD, Philips PW3830), measured with a glancing angle of 0.8 under Cu Kα radiation at 40 kV.

Micro-Raman measurements were performed with a Renishaw inVia Raman Microscope using 785 nm laser line with an acquisition time of 20 s, 0.4 mW power at the sample and a $50 \times$ ULWD objective; Rhodamine 6G (R6G) was chosen as SERS probe molecule. Prior to SERS experiments, the nanoporous gold samples were cleaned in concentrated nitric acid for 5 min and rinsed several times in de-ionized water. The samples were immersed in the aqueous solution of R6G with concentrations from 10^{-9} M to 10^{-6} M for one night, enabling the probe molecules to be adsorbed on the surface. Measurements were performed on the surface of sample after drying in air. All solutions were prepared from chemical grade reagents and de-ionized water. The Raman band of silicon wafer at 520 cm^{-1} was used to calibrate the spectrometer.

3. Results and discussion

Before chemical de-alloying, the as-sputtered Au-based nanoglass thin film (working pressure of 10 Pa) was observed by scanning electron microscopy (Fig.S1). The thin film had granular microstructure composed of grouped clusters with an average diameter of 14 nm, separated by less dense regions and voids in between. From the section view, the nanocolumns can be clearly distinguished. EDS results (Table S1) indicates that the composition of the thin films is comparable with that of the target. The XRD pattern (Fig.S5a) of as-sputtered nanoglass thin film contains characteristic broad halo around 40º, indicating its amorphous structure.

Figure 1 shows the typical morphologies of the de-alloyed nanoglass thin film at 70℃ for 30 min using various HNO_3 concentrations. In 1 M and 2 M HNO_3, the size of the ligament is small, around 30 nm, the distribution of ligaments is homogeneous showing the dissolution of less noble element occurs simultaneously under this

conditions. When the HNO_3 concentration increases to 5 M, the ligament size increases to ~40 nm (Fig.1c) and many large ligaments are distributed among smaller ones. The inhomogeneity of ligament size can be attributed to the local coarsening during the de-alloying process. As the HNO_3 concentration increase to 10 M, large ligaments are formed by extensive coarsening of crystals. The plot of ligament size as a function of HNO_3 concentration is provided in Fig.S1.

Figure S3 shows the surface morphologies of the samples de-alloyed in 1 M HNO_3 for 30 min at different temperatures. At 30℃, the less dense zones in between nanocolumns have been etched and ligaments start to form. When the electrolyte temperature increases to 50℃, the ligaments grow separately with homogeneous distribution. On increasing temperature the coarsening is apparent, and the ligament size increases from~14 nm (Fig.S3a) to ~45 nm (Fig.S3e) as the electrolyte temperature increases from 30 to 80℃. Compared with nanoporous gold de-alloyed from ribbons with the same composition, the ligament size is smaller under the same de-alloying conditions.
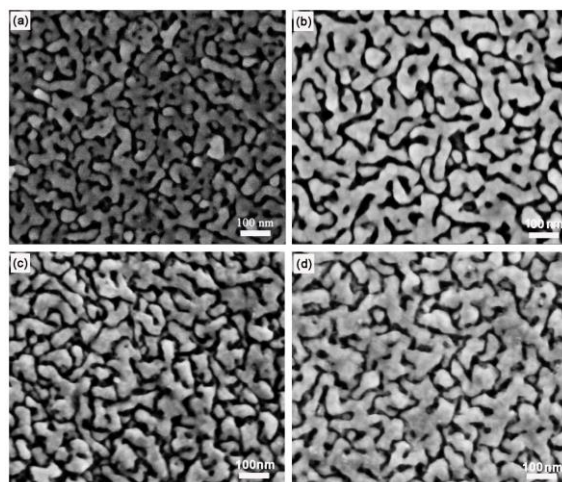

Figure 1. SEM images of nanoglass films after chemically de-alloying at 70℃ for 30 min in HNO_3 concentration of:(a) 1 M HNO_3, (b) 2 M HNO_3, (c) 5 M HNO_3 and (d) 10 M HNO_3.

Fig. 2 shows the microstructure evolution of $Au_{40}Cu_{28}Ag_7Pd_5Si_{20}$ nanoglass thin film at different de-alloying times from 5 min to 6 h in 1M HNO_3 at 70℃. Initially, the electrolyte disrupts the structure of the film penetrating into the columns from voids in between. The average ligament size is around 18 nm which is similar to the average size of the columns. When the de-alloying time increases (10 min), the ligaments grow and form through the whole thickness of the film as seen in cross section. After 30 min, the XRD reflections of face-centered cubic (fcc) Au appear (Fig.S5b). After de-alloying for 1 hour, the ligaments coalesce with each other and the XRD pattern (Fig.S5c) shows sharp peaks of fcc Au. The size of ligament increases from around 20 nm to 100 nm as de-alloying time increases to 2 hours (Fig.S4). Extending the de-alloying time to 6 hours, the morphology of ligaments is similar to that obtained by de-alloying metallic glass precursors in the form of ribbon, consisting of nanocrystals with random orientation and large nanopores. Compared with the amorphous ribbons,

faster de-alloying kinetics is confirmed due to the nanocolumnar structure with glassy interfaces around the dense glass regions where the electrolyte penetrates more easily. The percolation of the electrolyte through the interfaces results in atom removal not only from the top of the material but also from the lateral sides of nanocolumn.
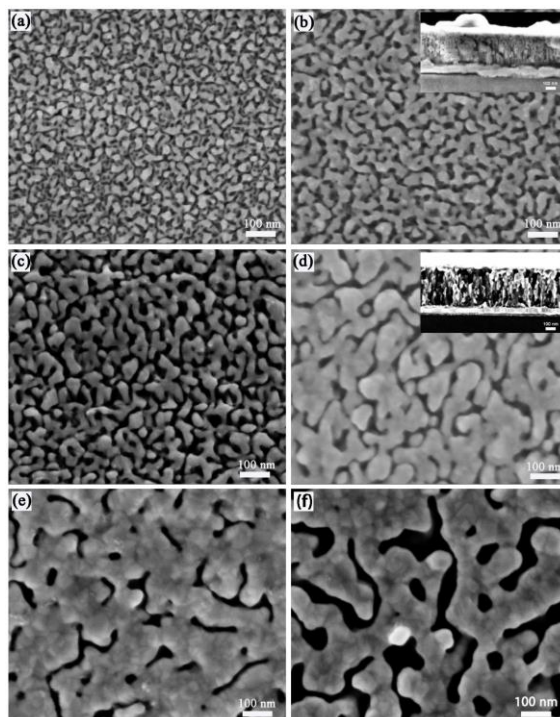

Figure 2. SEM images of nanoglass films after chemically de-alloyed in 1 M HNO$_3$ at 70℃ for (a) 5 min, (b) 10 min, (c) 30 min, (d) 1 h, (e) 2 h and (f) 6 h. The insets show the corresponding cross section.

A closer look into the ligament microstructure formed by de-alloying a Au-based nanoglass thin film in 1 M HNO$_3$ at 70°C for 15 min is provided by TEM observation. The images indicate that ligaments with an average size of 24±5nm are formed (Fig 3a), confirming the SEM images, while the lattice fringes are oriented in various directions. This observation confirms that the impingement of nanocrystals which are formed during de-alloying leads to a nanocrystalline network of rough ligaments [22].
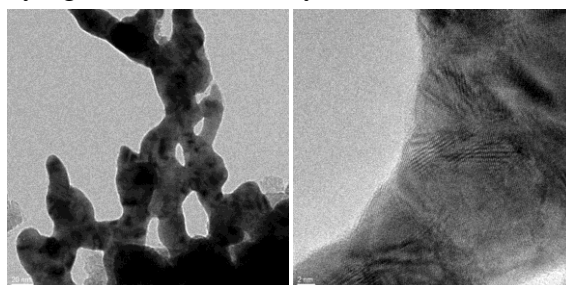

Figure 3. TEM images of the de-alloyed Au-based nanoglass thin film in 1 M HNO$_3$ at 70°C for 15 min. Samples were deposited employing the same sputtering parameters but without the Cr and Au adhesion layers in order to detach them easily from the glass substrate after de-alloying and observe them in TEM without cutting or thinning.

XPS measurements were performed to reveal the chemical composition at the top surface of film and to estimate the residual sacrificial elements left after de-alloying 1M HNO_3 at 70 °C with different times. The results are displayed in Table S2. After de-alloying for 30 min, XPS results reveal that the Cu content on the top surface of the film decreased sharply. The Si content remains high, however, the Si element is concentrated in silica patches (gray shadows in SEM images) which do not hinder the penetration of the electrolyte into the pores. With continuation of the de-alloying process, the Au content increases and the Cu and Si content decrease. A small amount of Ag was detected in all sample surfaces.

The SERS capability of the nanoporous gold thin film was examined using Rhodamine 6G (R6G) as probe molecule. Figure 4(a) shows the SERS spectra collected with samples de-alloyed in 1 M HNO_3 at 70℃ for different times after one night immersion in 10^{-6} M R6G solution. The SERS spectra display the characteristic peaks of R6G at Raman shift of 1653, 1513 and 1365 cm^{-1}, which are attributed to the symmetric modes of the in-plane C-C stretching vibrations. The Raman band at 1312 and 1186 cm^{-1} are associated with the N-H and C-H in-plane bend vibrations, respectively. The Raman band at 774 and 612 cm^{-1} are assigned to the C-H out-of-plane and C-C-C ring in-plane bending vibrations [37]. No visible Raman band of R6G molecules is detected using the sample de-alloyed for 30 min. This was only partially de-alloyed (Fig.S5b) therefore the SERS active sites were not available yet. After 1 h de-alloying, ligaments and pores are well formed. The main Raman bands of R6G can be observed with obvious enhanced SERS activity. Increasing the de-alloying time to 2 h, the SERS intensity of R6G is around 5 times higher than the one found after de-alloying for 1 h. Extending the de-alloying time to 6 h the SERS intensity decreases, which may be attributed to the large ligament size. It was recognized that the strong SERS enhancement of nanoporous materials was mainly due to the electromagnetic effect arising from the resonant excitation of localized surface plasmons in the vicinity of the ligaments and nanopores[38,39]. The electromagnetic coupling effect between adjacent gold ligaments give rise to the significant enhancement of the electromagnetic field intensity[40]. Moreover, when the nanoporous gold is prepared from amorphous alloy, spontaneous germination and growth of crystals rich in the noble element occurs to form ligaments. Therefore, the ligaments are constituted by several nanocrystals with numerous kinks and step edges, separated by grain boundaries (Fig. 3) which may further enhance the localized electromagnetic field.

In order to test the SERS sensitivity, the Raman spectra for R6G concentrations varying from 10^{-9} M to 10^{-6} M on the sample de-alloyed in 1 M HNO_3 at 70℃ for 2 h were collected and shown in Figure 4(b). At 10^{-8} M, the main characteristic peaks of R6G at 1513, 1365, and 1312 cm^{-1} could still be detected; this is taken as the detection limit for R6G adsorbed on the present nanoporous gold thin film. The SERS intensities of the peaks at 1513, 1265, and 1312 cm^{-1} as a function of R6G concentration for this sample are plotted in Fig. 4(c). A SERS intensity map using the

1312 cm^{-1} vibration mode with R6G concentration of 10^{-7} M on nanoporous gold samples was collected(Fig.4d). The whole mapping area was 48×48 μm^2 with the step length of 4 μm. This measurement clearly demonstrates the presence of plasmonic "hot spots" with not completely homogenous distribution across the nanoporous microstructure.
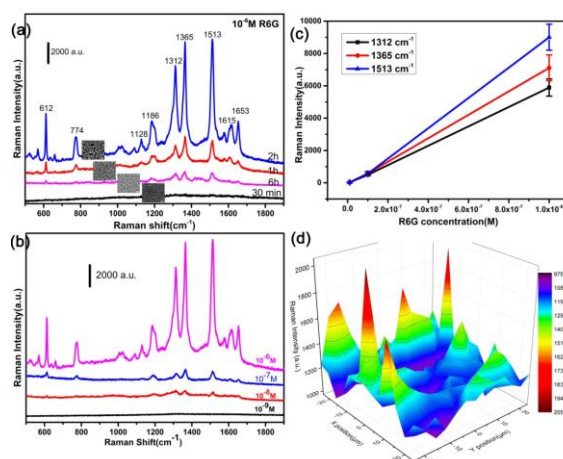

Figure 4. (a) SERS spectra of R6G on nanoporous gold thin films at different de-alloying times (b) SERS spectra of R6G at different concentrations on sample de-alloyed in 1 M HNO$_3$ at 70℃ for 2 h. (c) Raman intensity at 1312 cm^{-1}, 1365 cm^{-1} and 1513 cm^{-1} as a function of R6G concentrations (in logarithmic scale). The error bars were calculated from at least five measurements on random spots on the same substrate. (d) SERS intensity mapping image of 48×48 μm^2 at the step length of 4 μm with R6G concentration of 10^{-7} M centered on characteristic peak at 1312 cm^{-1}. The laser wavelength was 785 nm with an acquisition time of 20 s.

4. Conclusion

In summary, nanoporous gold films have been prepared by chemical de-alloying a Au based nanoglass with nanocolumnar structure, $Au_{40}Cu_{28}Ag_7Pd_5Si_{20}$(at.%), which was prepared by magnetron sputtering. Gold ligaments ranging from 20 to 100nm were obtained by adjusting the de-alloying parameters, such as de-alloying time, HNO$_3$ concentration and electrolyte temperature. The nanoporous gold thin film gives rise to surface enhanced Raman scattering capability using Rhodamine 6G as probe molecule. A low detection limit down to 10^{-8} M for R6G was achieved and the SERS enhancement is attributed to the localized enhanced electromagnetic fields around nano-sized ligaments and the electromagnetic coupling between ligaments.

Acknowledgements

References

[1]   S. Schlücker, Angew. Chemie - Int. Ed. 53 (2014) 4756–4795.

[2]   L.A. Lane, X. Qian, S. Nie, Chem. Rev. 115 (2015) 10489–10529.

[3]   S. Nie, S.R. Emory, Science. 275 (1997) 1102–1106.

[4]   K. Kneipp, Y. Wang, H. Kneipp, L.T. Perelman, I. Itzkan, R.R. Dasari, M.S. Feld, Phys. Rev. Lett. 78 (1997) 1667–1670.

[5]   P.L. Stiles, J.A. Dieringer, N.C. Shah, R.P. Van Duyne, 1 (2008) 601–626.

[6]   S. Ding, J. Yi, J. Li, B. Ren, D. Wu, R. Panneerselvam, Z. Tian, Nat. Rev. Mater. 1 (2016) 16021.

[7]   Q. Zhang, Y. Zhou, E. Villarreal, Y. Lin, S. Zou, H. Wang, Nano Lett. 15 (2015) 4161–4169.

[8]   M.P. Cecchini, V. a Turek, J. Paget, A. a Kornyshev, J.B. Edel, Nat. Mater. 12 (2012) 165–171.

[9]   F. De Angelis, F. Gentile, F. Mecarini, G. Das, M. Moretti, P. Candeloro, M.L. Coluccio, G. Cojoc, a. Accardo, C. Liberale, R.P. Zaccaria, G. Perozziello, L. Tirinato,   a. Toma, G. Cuda, R. Cingolani, E. Di Fabrizio, Nat. Photonics 5 (2011) 682–687.

[10]   H. Liu, L. Zhang, X. Lang, Y. Yamaguchi, H. Iwasaki, Y. Inouye, Q. Xue, M. Chen, Sci. Rep. 1 (2011) 1–5.

[11]   L. Zhang, X. Lang, A. Hirata, M. Chen, ACS Nano 5 (2011) 4407–4413.

[12]   H. Qiu, X. Li, H. Xu, H. Zhang, Y. Wang, J. Mater. Chem. C Mater. Opt. Electron. Devices 2 (2014) 9788–9799.

[13]   J. Erlebacher, M.J. Aziz,   a Karma, N. Dimitrov, K. Sieradzki, Nature 410 (2001) 450–453.

[14]   I. Mccue, E. Benn, B. Gaskey, J. Erlebacher, Annu. Rev. Mater. Res. 46 (2015) 1–24.

[15]   Y. Ding, Y.J. Kim, J. Erlebacher, Adv. Mater. 16 (2004) 1897–1900.

[16]   L.H. Qian, M.W. Chen, Appl. Phys. Lett. 91 (2007) 83105.

[17]   M. Zhang, A.M. Jorge Junior, S.J. Pang, T. Zhang, A.R. Yavari, Scr. Mater. 100 (2015) 21–23.

[18]   E.-M. Steyskal, Z. Qi, P. Pölt, M. Albu, J. Weissmüller, R. Würschum, Langmuir 32 (2016) 7757–7764.

[19]   R. Li, X. Liu, H. Wang, Y. Wu, Z.P. Lu, Corros. Sci. 104 (2016) 227–235.

[20]   E.M. Paschalidou, F. Scaglione, A. Gebert, S. Oswald, P. Rizzi, L. Battezzati, J. Alloys Compd. 667 (2016) 302–309.

[21]   J. Yu, Y. Ding, C. Xu, A. Inoue, T. Sakurai, M. Chen, Chem. Mater. 20 (2008) 4548–4550.

[22]   E.M. Paschalidou, F. Celegato, F. Scaglione, P. Rizzi, L. Battezzati, A. Gebert, S. Oswald, U. Wolff, L. Mihaylov, T. Spassov, Acta Mater. 119 (2016) 177–183.

[23]   J. Jing, A. Krämer, R. Birringer, H. Gleiter, U. Gonser, J. Non. Cryst. Solids 113 (1989) 167–170.

[24]   H. Gleiter, Acta Mater. 56 (2008) 5875–5893.

[25]   J.X. Fang, U. Vainio, W. Puff, R. Würschum, X.L. Wang, D. Wang, M. Ghafari, F. Jiang, J. Sun, H. Hahn, H. Gleiter, Nano Lett. 12 (2012) 458–63.

[26]   R. Morrish, K. Dorame, A.J. Muscat, Scr. Mater. 64 (2011) 856–859.

[27]   E.J. Gwak, N.R. Kang, U.B. Baek, H.M. Lee, S.H. Nahm, J.Y. Kim, Scr. Mater. 69 (2013) 720–723.

[28]   G. Pia, M. Mascia, F. Delogu, Scr. Mater. 76 (2014) 57–60.

[29]   P. Daggumati, Z. Matharu, L. Wang, E. Seker, Anal. Chem. 87 (2015) 8618–8622.

[30]   V.A. Online, O. Kurtulus, P. Daggumati, E. Seker, Nanoscale 6 (2014) 7062–7071.

[31]   O. Polat, E. Seker, J. Phys. Chem. C 119 (2015) 24812–24818.

[32]   V.A. Online, F. Zhao, J. Zeng, P. Sun, J. Qi, P. Motwani, M. Gheewala, C. Li, A. Paterson, U. Strych, B. Raja, R.C. Willson, J.C. Wolfe, T.R. Lee, W. Shih, Nanoscale 6 (2014) 8199–8207.

[33]   T.R. Lee, W. Shih, RSC Adv. 4 (2014) 36682–36688.

[34]   J. Zeng, F. Zhao, M. Li, C.-H. Li, T.R. Lee, W.-C. Shih, J. Mater. Chem. C 3 (2014) 247–252.

[35]   J. Qi, P. Motwani, M. Gheewala, C. Brennan, J.C. Wolfe, W. Shih, Nanoscale 5 (2013) 4105.

[36]   H. Guo, W. Zhang, C. Qin, J. Qiang, M. Chen, A. Inoue, Mater. Trans. 50 (2009) 1290–1293.

[37]   F. Der Mai, C.C. Yu, Y.C. Liu, C.C. Chang, K.H. Yang, J. Electroanal. Chem. 712 (2014) 96–102.

[38]   X.Y. Lang, L.Y. Chen, P.F. Guan, T. Fujita, M.W. Chen, Appl. Phys. Lett. 94 (2009) 10–13.

[39]   C. Li, Ö. Dag, T.D. Dao, T. Nagao, Y. Sakamoto, T. Kimura, O. Terasaki, Y. Yamauchi, Nat. Commun. 6 (2015) 6608.

[40]   X. Lang, P. Guan, L. Zhang, T. Fujita, M. Chen, J. Phys. Chem. C 113 (2009) 10956–10961.

[41]   Y. Xue, F. Scaglione, E.M. Paschalidou, P. Rizzi, L. Battezzati, Chem. Phys. Lett. 665 (2016) 6–9.